

Chapter 4

DESIGN AND SIMULATIONS OF PHOTONIC RESONATORS

This chapter explains why silicon is a good material for near IR wavelength photonic devices at low temperature. The basic theory of finite difference time domain (FDTD) simulations is explained. Then the entire FDTD simulation procedure is described, which is used to determine the parameters for Si ring resonators on SiC.

4.1 Silicon photonic devices for near IR wavelength

The emission of qubits can be improved by using scalable on-chip cavity devices that couple to the optical transition to generate lifetime limited emission and channel it into optical waveguides. One strategy to develop on-chip photonic devices is to fabricate them directly in the qubit host material. For this technique, it is required to start with thin membranes on a low refractive index substrate, or on a substrate that can be etched away or undercut. Even if some techniques exist to produce membranes, it is not always the case that these membranes can host high quality quantum emitters. Additionally, fabrication process often damages the material and leaves unwanted charges that degrades qubits' properties. For 4H-SiC, heteroepitaxial growth is not available and creating thin membranes is not straightforward. An alternative is to make hybrid devices in a high refractive index layer located on top of the substrate hosting the qubits, such that the emitters are coupled to the evanescent field. In my research project, we used a crystalline silicon (c-Si) hybrid platform of ring resonators and waveguides fabricated on top of SiC substrate shown in figure 4.1.

We want to choose the right device layer material for the hybrid platform. We can check if the material has large enough refractive index contrast to possibly confine light well and if it has minimal absorption for the wavelength range of interest. The intrinsic quality factor of the Si ring resonator surrounded by air is calculated for different temperature as shown in figure 4.2. This is calculated based on absorption

coefficient of Si [70, 71] and resonator theory [72, 73]:

$$a^2 = e^{-\alpha L} \quad (4.1)$$

$$FWHM = \frac{\Delta\theta\lambda_{res}^2}{\pi n_{eff}L - \lambda_{res}\Delta\theta} \quad (4.2)$$

$$\Delta\theta = \cos^{-1}\left(2 - \frac{1 + a^2|t_1|^2|t_2|^2}{2a|t_1||t_2|}\right) \quad (4.3)$$

a is single round amplitude transmission and α is absorption coefficient. L is the round trip length. t_1 and t_2 are self-coupling coefficient for two waveguides. λ_{res} is the resonant wavelength. n_{eff} is the effective refractive index. These intrinsic quality factor values correspond to silicon ring resonators with perfectly smooth surfaces (no scattering loss) with material absorption loss, characterized by a single round amplitude transmission a . Silicon has a bandgap at 1.11 eV (1120 nm wavelength of light) at 300K [74]. At lower temperature the bandgap decreases and silicon has less interband absorption. From the figure 4.2, at 1050 nm and 20K the intrinsic quality factor exceeds 10^8 . At this low temperature Si shows sufficient transparency to be used as a device layer coupling divacancy ZPLs ranging in the interval 1080-1130 nm.

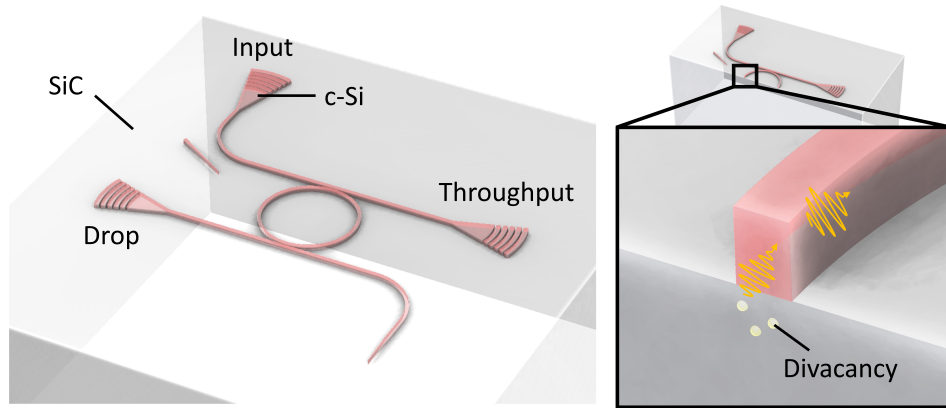


Figure 4.1: Left: c-Si ring resonator on 4H-SiC for spin-photon interfaces. c-Si is drawn in red, while the transparent part underneath is 4H-SiC. Right: Cross section showing the ring resonator near color centers in the 4H-SiC underneath it, that can couple to the evanescent field of the cavity.

4.2 Principles of finite-difference time-domain (FDTD) method

The finite-difference time-domain (FDTD) method is a systematic computational method for electromagnetic fields using the central difference approximation of

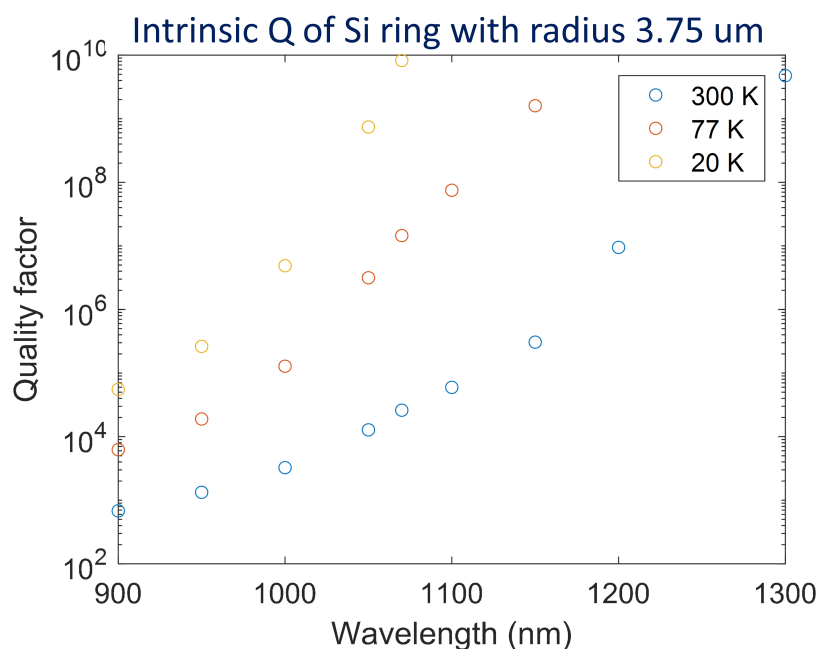


Figure 4.2: Intrinsic quality factor of Si ring resonator surrounded by air at different temperature.

coupled Maxwell's curl equations (Faraday's law and Ampere's law) [75]. Space and time is divided into grids, which is called Yee lattice to update the results of both electric and magnetic field at certain location/time to those of neighbor location/time. In an actual simulation, computation starts in a volume with finite grids in space at time zero and, using initial condition of electric or magnetic field, the field value at the neighbor grid in space at next time step will be calculated. This continues until all field values at that time step of interest are computed. Then time is incremented by one time step and the field calculation for the same region starts again.

If we consider an electromagnetic (EM) wave in isotropic media, the electric displacement field \mathbf{D} and auxiliary magnetic field \mathbf{H} are parallel to electric field \mathbf{E} and magnetic field \mathbf{B} accordingly.

$$\mathbf{D} = \varepsilon \mathbf{E} \quad (4.4)$$

$$\mathbf{B} = \mu \mathbf{H} \quad (4.5)$$

where ε is electric permittivity and μ is magnetic permeability. The Maxwell's curl

equations in isotropic media can be written as:

$$\nabla \times \mathbf{E} + \mu \frac{\partial \mathbf{H}}{\partial t} = 0 \quad (4.6)$$

$$\nabla \times \mathbf{H} - \varepsilon \frac{\partial \mathbf{E}}{\partial t} = \mathbf{J} \quad (4.7)$$

Each component of the electric field and auxiliary magnetic field is written,

$$\frac{\partial E_x}{\partial t} = \frac{1}{\varepsilon} \left(\frac{\partial H_z}{\partial y} - \frac{\partial H_y}{\partial z} - J_x \right) \quad (4.8)$$

$$\frac{\partial E_y}{\partial t} = \frac{1}{\varepsilon} \left(\frac{\partial H_x}{\partial z} - \frac{\partial H_z}{\partial x} - J_y \right) \quad (4.9)$$

$$\frac{\partial E_z}{\partial t} = \frac{1}{\varepsilon} \left(\frac{\partial H_y}{\partial x} - \frac{\partial H_x}{\partial y} - J_z \right) \quad (4.10)$$

$$\frac{\partial H_x}{\partial t} = \frac{1}{\mu} \left(\frac{\partial E_z}{\partial y} - \frac{\partial E_y}{\partial z} \right) \quad (4.11)$$

$$\frac{\partial H_y}{\partial t} = \frac{1}{\mu} \left(\frac{\partial E_x}{\partial z} - \frac{\partial E_z}{\partial x} \right) \quad (4.12)$$

$$\frac{\partial H_z}{\partial t} = \frac{1}{\mu} \left(\frac{\partial E_y}{\partial x} - \frac{\partial E_x}{\partial y} \right) \quad (4.13)$$

where \mathbf{J} is the electric current density. According to the Yee algorithm[75, 76], if we denote any function evaluated at a grid point in space and time with lattice increment $(\Delta x, \Delta y, \Delta z, \Delta t)$ in x, y, z and t coordinates,

$$u|_{i,j,k}^n = u(i\Delta x, j\Delta y, k\Delta z, n\Delta t) \quad (4.14)$$

the partial differential equations of time are approximated using centered finite difference expressions at a space point (i, j, k):

$$\frac{\partial u|_{i,j,k}^n}{\partial t} = \frac{u|_{i,j,k}^{n+\frac{1}{2}} - u|_{i,j,k}^{n-\frac{1}{2}}}{\Delta t} + O[(\Delta t)^2] \quad (4.15)$$

Partial differential equations of space coordinates can be approximated in similar manner. As an example, using this approximation on equation 4.10, it can be written as following:

$$E_z|_{i,j,k}^{n+\frac{1}{2}} = \frac{\Delta t}{\varepsilon} \left(\frac{H_y|_{i+\frac{1}{2},j,k}^n - H_y|_{i-\frac{1}{2},j,k}^n}{\Delta x} - \frac{H_x|_{i,j+\frac{1}{2},k}^n - H_x|_{i,j-\frac{1}{2},k}^n}{\Delta y} - J_z|_{i,j,k}^n \right) + E_z|_{i,j,k}^{n-\frac{1}{2}} \quad (4.16)$$

As we can see from this equation, E_z is approximated by a combination of H_x and H_y at a half previous time step and E_z at the previous time step. Now we want to know how to approximate H_x and H_y using equations 4.11, 4.12, and 4.15.

$$H_x|_{i,j+\frac{1}{2},k}^n = \frac{\Delta t}{\varepsilon} \left(\frac{E_z|_{i,j+1,k}^{n-\frac{1}{2}} - E_z|_{i,j,k}^{n-\frac{1}{2}}}{\Delta y} - \frac{E_y|_{i,j+\frac{1}{2},k+\frac{1}{2}}^{n-\frac{1}{2}} - E_y|_{i,j+\frac{1}{2},k-\frac{1}{2}}^{n-\frac{1}{2}}}{\Delta z} \right) + H_x|_{i,j+\frac{1}{2},k}^{n-1} \quad (4.17)$$

$$H_y|_{i+\frac{1}{2},j,k}^n = \frac{\Delta t}{\varepsilon} \left(\frac{E_x|_{i+\frac{1}{2},j,k+\frac{1}{2}}^{n-\frac{1}{2}} - E_x|_{i+\frac{1}{2},j,k-\frac{1}{2}}^{n-\frac{1}{2}}}{\Delta z} - \frac{E_z|_{i+1,j,k}^{n-\frac{1}{2}} - E_z|_{i,j,k}^{n-\frac{1}{2}}}{\Delta x} \right) + H_y|_{i+\frac{1}{2},j,k}^{n-1} \quad (4.18)$$

As a further example, we write down E_x component used in H_x above:

$$E_x|_{i+\frac{1}{2},j,k+\frac{1}{2}}^{n-\frac{1}{2}} = \frac{\Delta t}{\varepsilon} \left(\frac{H_z|_{i+\frac{1}{2},j+\frac{1}{2},k+\frac{1}{2}}^{n-1} - H_z|_{i+\frac{1}{2},j-\frac{1}{2},k+\frac{1}{2}}^{n-1}}{\Delta y} - \frac{H_y|_{i+\frac{1}{2},j,k+1}^{n-1} - H_y|_{i+\frac{1}{2},j,k}^{n-1}}{\Delta z} \right) - J_x|_{i+\frac{1}{2},j,k+\frac{1}{2}}^{n-1} + E_x|_{i+\frac{1}{2},j,k+\frac{1}{2}}^{n-\frac{3}{2}} \quad (4.19)$$

You can see the half step coordinate offset between electric field and magnetic field component in these equations. With centered difference approximation, each electric field and magnetic field component lie at a different 3D spatial lattice point offset by half of the increment, in order to update them in time sequence. Also, the time step is half of the increment different for electric and magnetic field. This is shown in figure 4.3.

4.3 Comparison with other EM simulation method

Finite element method (FEM)

FEM replaces the Maxwell equations in continuous space with simpler interpolation functions in smaller subspaces (elements). By doing this, functions with infinite degree of freedom can be approximated by solving finite coefficients of simpler functions. The first step is discretization of the space that will be simulated. The entire space is divided into small elements that can take shapes of triangles or rectangles etc. in 2D, tetrahedra or rectangular blocks etc. in 3D. The size and distribution of the elements are carefully decided so that the numerical approximations

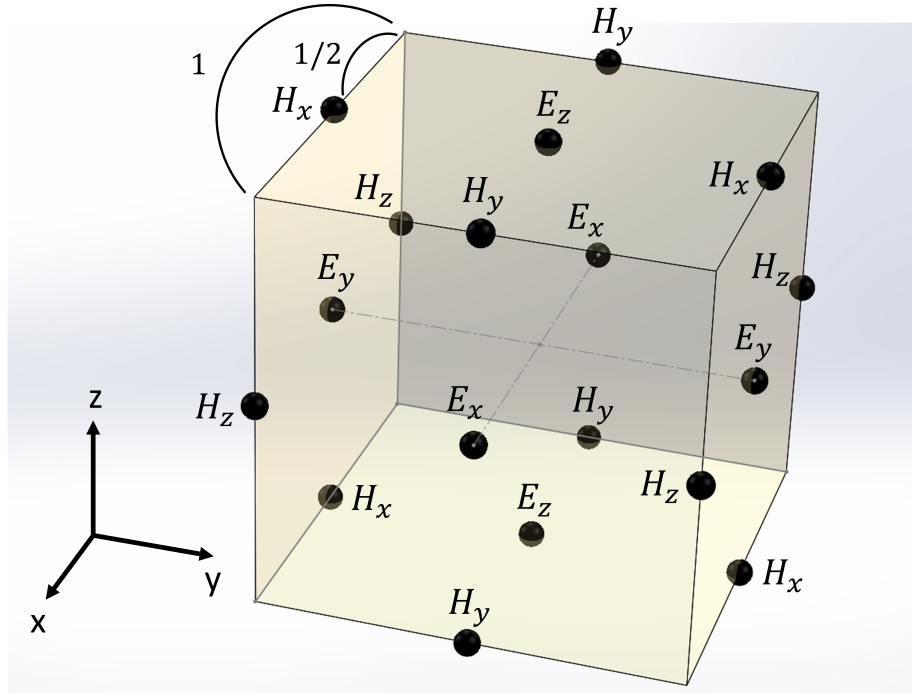


Figure 4.3: Electric and magnetic component positions in Yee algorithm.

are sufficiently accurate with appropriate computation time. The principle is that electromagnetic waves behave in a way that they minimize their total energy. FEM is used in COMSOL Multiphysics software offered by COMSOL, Inc.

4.4 MEEP simulation of c-Si on SiC ring resonator devices

We used the open-source software MEEP[77] to simulate our Si ring resonator devices on SiC with FDTD method. This section explains details of the MEEP simulation steps. These simulations were run in multi-core computers using the parallel computing version of MEEP, meep-mpi. The most time consuming simulation described in the section is a 3D ring simulation with waveguide, typically taking 2-3 hours with 20 processors.

2D cylindrical ring simulation

In this first simulation step, we want to simulate ring resonators by looking at the modes confined in a 2D space assuming cylindrical symmetry. We'd like to choose the ring's radius, width and height at the end of the simulation step. We prefer

smaller ring radius (smaller mode volume), smaller ring height (More evanescent field underneath the substrate) and high quality factor. We wanted to simulate single TM mode ring resonator. The refractive index configuration is shown in figure 4.4 (a). TM mode was chosen because stronger field can exist beneath the Si and SiC interface compared to the transverse electric mode due to the field discontinuity, which is shown in figure 4.4 (b)(c). This simulates the ring structure without any waveguide. Because it has continuous rotational symmetry, one dimension in ϕ is reduced and we can only think about field change in r and z coordinates. In MEEP, you can evaluate the quality factor by using special harmonic inversion function at a given point inside the ring. The simulated quality factor vs. ring radius with a fixed height 360 nm and width 300 nm is shown in figure 4.5. One can see more light leaking out through the substrate to the external ring direction when the radius of the ring is smaller. In this ring design, the radiation limit was reached with radius $\sim 3.25 \mu\text{m}$ with simulated $Q < 1000$. The radius $3.75 \mu\text{m}$ with simulated Q was chosen to minimize the ratio of the quality factor $Q = 7 \times 10^5$ to mode volume V considering that the quality factor in the current fabricated devices is limited by scattering losses to $Q = 23000$. The simulation gives a calculated V of $19.5 (\lambda_{ZPL}/n_{Si})^3$. The 2D cylindrical ring simulation code is attached in the appendix ??.

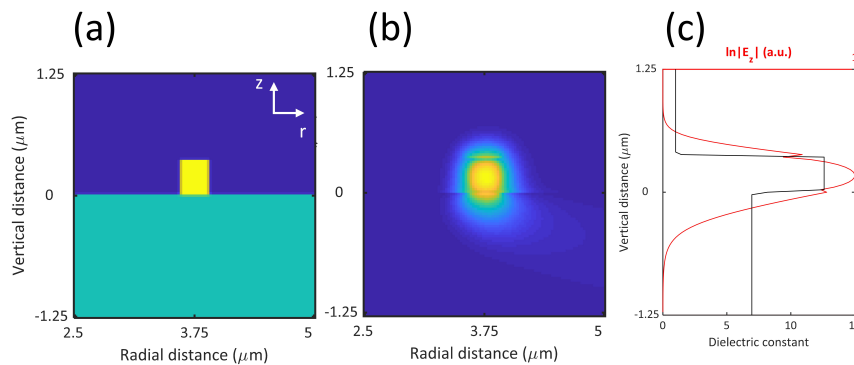


Figure 4.4: 2D cylindrical ring simulation (a) Refractive index setting (green: SiC/ $n=2.64$, yellow: Si/ $n=3.55$ and blue: air/ $n=1.00$)(b) $\ln|E_z|$ with colormap(c) Plot of $\ln|E_z|$ at the ring width center cross section.

3D ring simulation

3D ring simulation is necessary if we introduce waveguides that guide light to grating couplers. In contrast to 2D ring simulation with perfectly smooth sidewalls, roughness on rings is inevitable because of the computational grids (i.e. the resolution). In typical resolution of 40 pixels per unit length, 1 μm used in these simulation, the

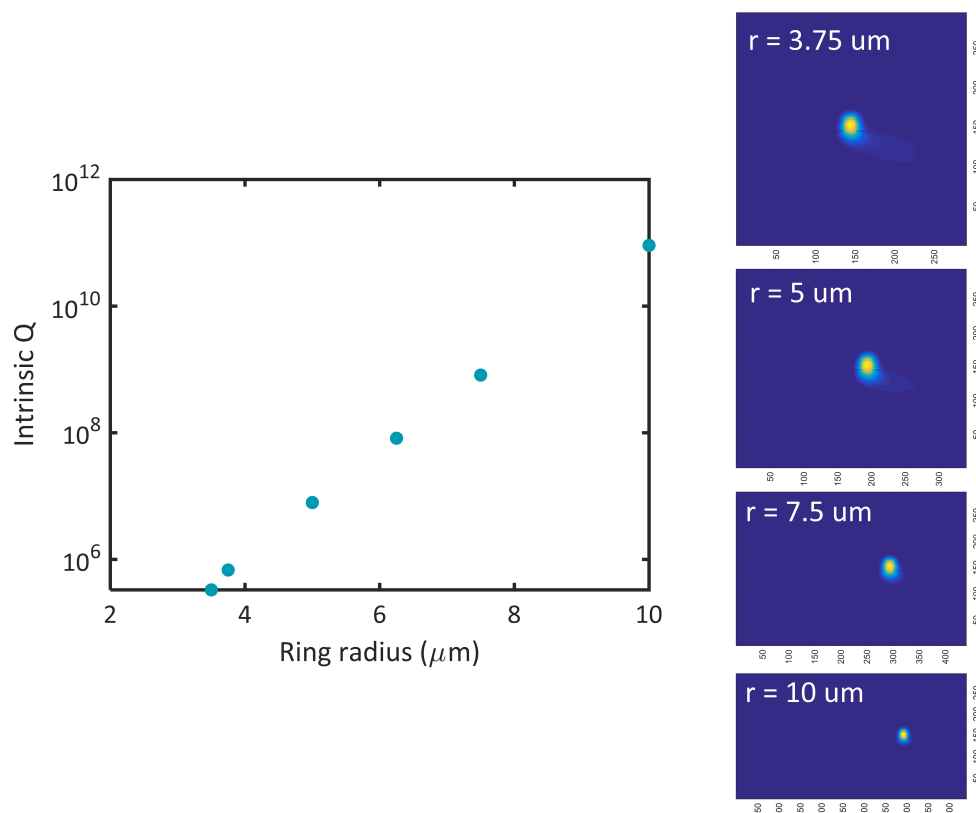


Figure 4.5: 2D cylindrical ring simulation quality factor vs. ring radius with height 360 nm and width 300 nm.

refractive index assignment causes rough radial surfaces with roughness of order ~ 10 nm. So we should consider the simulated quality factor in 3D a lower bound of that of fabricated ring resonators only with scattering effect. To fabricate close to critically coupled ring resonators, we simulated ring resonators with waveguides at different distances from rings. The typical simulation setup and results are shown in figure 4.6 (a)(b). The change in quality factor depending on waveguide-ring distance is shown in figure 4.6 (c). The intrinsic quality factor in this 3D simulation was 2.1×10^5 . From this result, we choose to fabricate arrays of ring resonators with different waveguide separation that gives 20-80% of intrinsic quality factor. The 3D ring-waveguide simulation code is attached in the appendix ??.

2D and 3D grating coupler simulation

To efficiently collect and detect emission from the divacancies grating couplers were added to the end of waveguides for diffracting light to a microscope objective. Basic

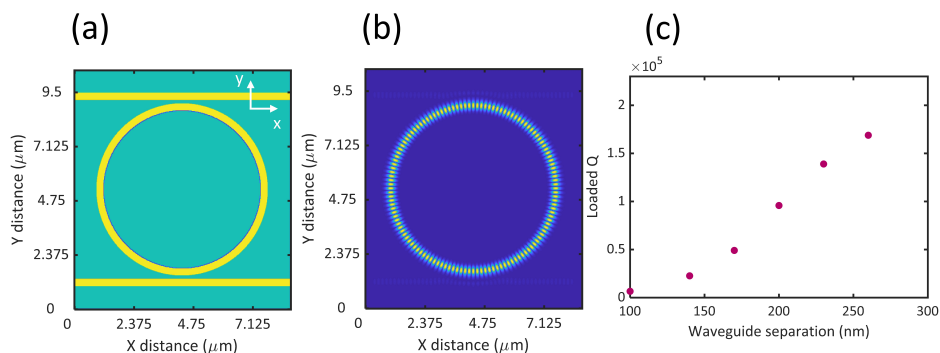


Figure 4.6: 3D ring simulation with waveguides. (a)Refractive index setting (color distribution same with figure 4.4) (b) $\ln|E_z|$ (c)Quality factor vs. waveguide distance

grating coupler parameters such as grating period and duty cycle were simulated for wavelength 1080 nm. To calculate the grating coupler efficiency we place a flux region in the simulated space where the fields are scattered and evaluate the electromagnetic flux or integral of Poynting vector going through that region. The following figure 4.7 depicts the typical simulation setup in 2D. The two lines are the flux regions in this simulation for evaluating diffracted light in almost vertical or angled direction accordingly. Also, a waveguide transmission simulation is performed to evaluate the flux going through the end of the waveguide, which is set to the same length of grating coupler in the other simulation. The grating coupler efficiency in these simulations is calculated by the normalization flux (F1) divided by the sum of the flux going through vertical/angled direction (F2+F3) in the grating coupler simulation, as shown in figure 4.7. In 2D simulations, gratings were considered to be straight and infinitely long in z direction.

I started the flux simulations by sweeping the grating period and duty cycle to find a parameter range that gives significant amount of F2 flux and a good wave profile. Our objective lens can collect light from a light cone of angle less than $\sim 38^\circ$, so we also wanted to pick parameters that ensure the grating doesn't diffract significantly beyond that angle. Then we simulated the flux in a finer sweep of parameters in this range and also took electric field output snapshots at the end of the simulation. The summary of the flux simulations with the finer sweep is shown in figure 4.8. We needed to look at the electric field diffraction pattern by plotting the snapshot to make sure the grating actually diffracts. Even if there seems to be a lot of flux going through F2, light might be scattered with the first grating without propagating

much. We wanted to see plane wave like pattern similar to what is shown in the right bottom figure 4.7. In this design of simple grating couplers, increasing the duty cycle with fixed period increases diffraction angle (figure 4.9) and increasing period with fixed duty cycle also increases diffraction angle (figure 4.10). This trend can be seen in the right panel of figure 4.8 by F2/F3 flux. To ensure the diffraction angle is not too steep I chose parameters with $F2/F3 > 10$ and F2 is close to maximum in the left panel of 4.8. From this simulation we picked grating parameters of grating period 470 nm and duty cycle 82 % (Grating width 385 nm and gap 85 nm) for fabrication.

3D simulations use concentric grating couplers, that are implemented in fabrication to see changes in efficiency compared to straight gratings. The 3D simulation configuration is shown in figure 4.11. The simulation revealed the concentric design doesn't change much the optimized parameters obtained in 2D simulation. The best parameters obtained from 3D simulation is period 490 nm and duty cycle 80 %. The 2D/3D simulation codes are included in appendix ??.

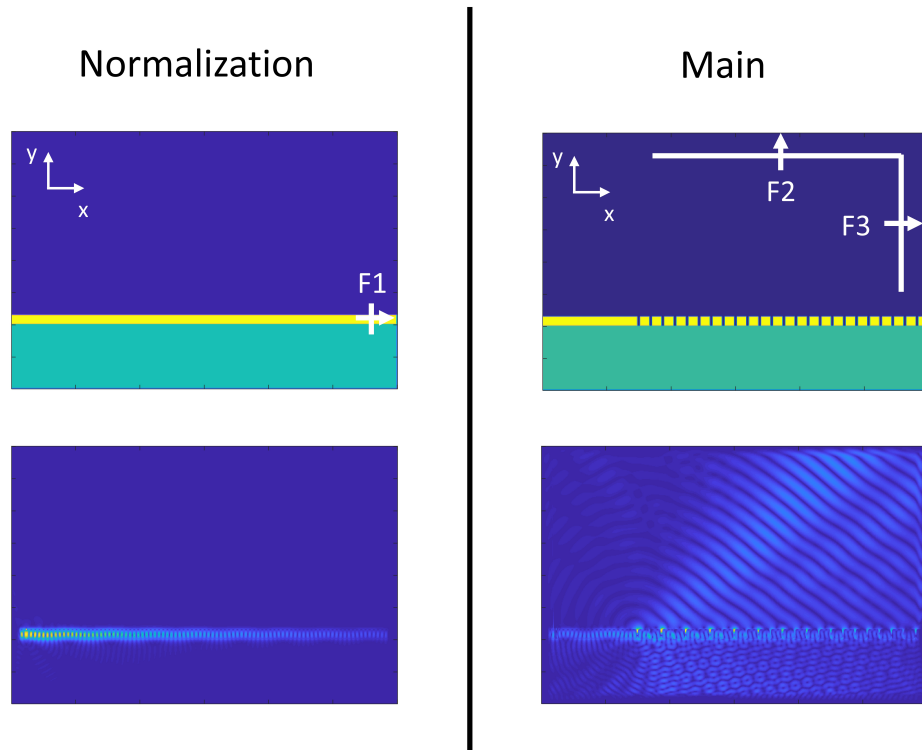


Figure 4.7: 2D grating simulation normalization simulation on the left. Main simulation is on the right. Top figures are refractive index configuration and bottom figures are plotting $\ln|E|$.

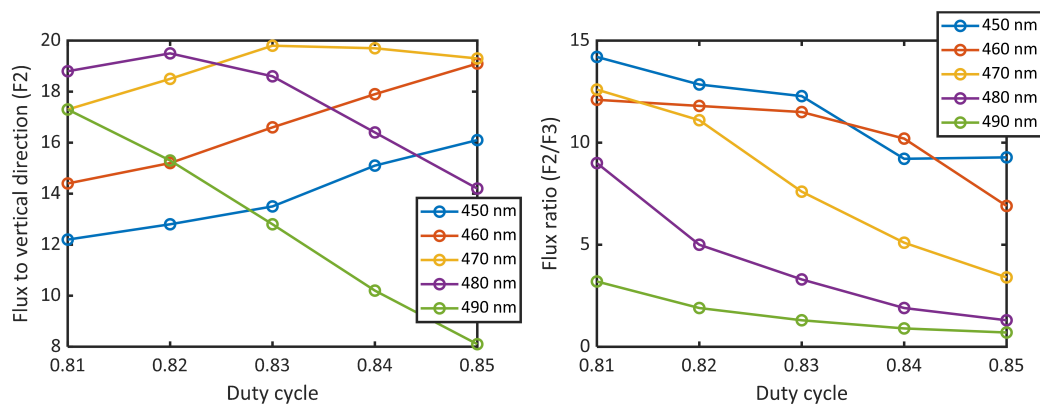


Figure 4.8: 2D grating flux depending on period and duty cycle.

Period 470 nm

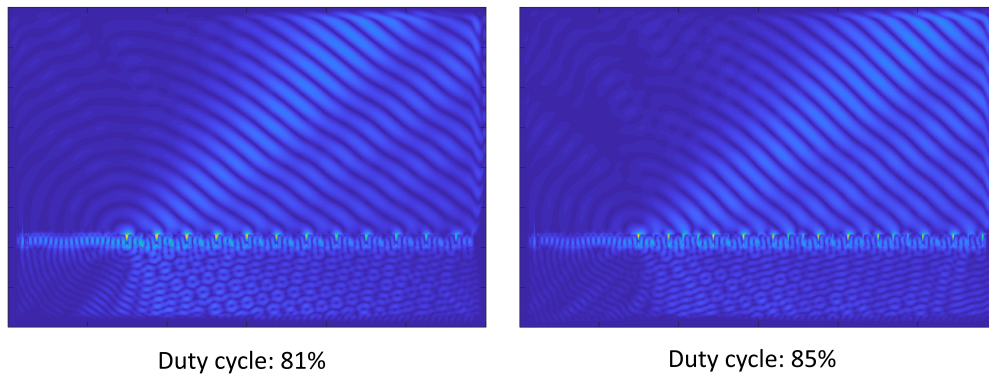


Figure 4.9: 2D grating diffraction angle change depending on duty cycle (fixed period)

Duty cycle 82%

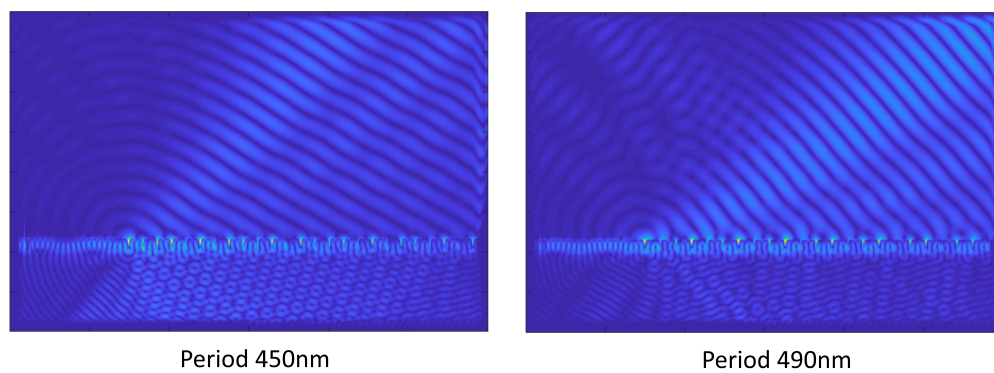


Figure 4.10: 2D grating diffraction angle change depending on period (fixed duty cycle)

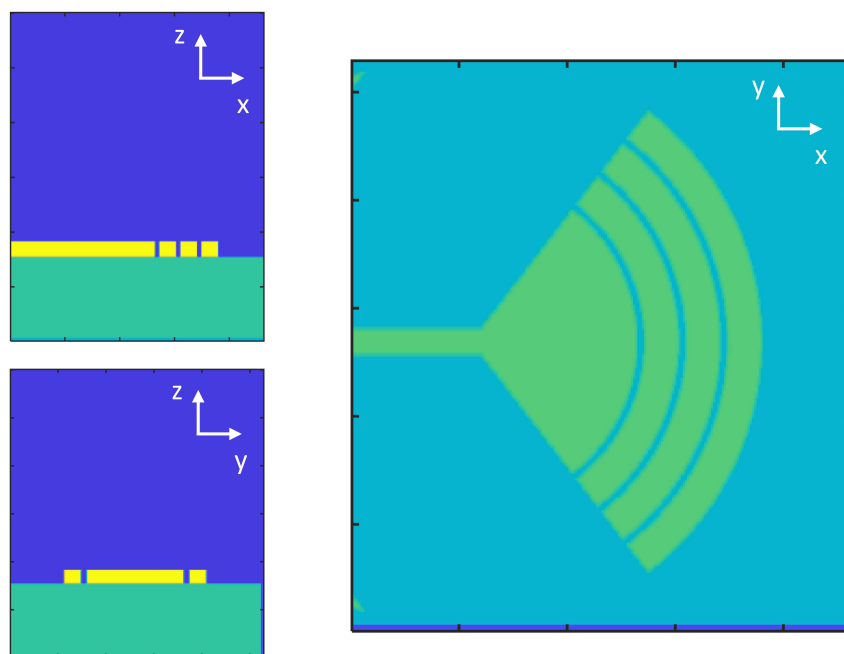


Figure 4.11: 3D grating simulation configuration. Each figure is at the center plane of the simulated space.